THE JOURNAL OF BIOLOGICAL CHEMISTRY VOL. 283, NO. 51, pp. 35983–35995, December 19, 2008

Structure of the Yeast Vacuolar ATPase*[S]

Received for publication, July 14, 2008, and in revised form, October 15, 2008 Published, JBC Papers in Press, October 27, 2008, DOI 10.1074/jbc.M805345200

Zhenyu Zhang[‡1], Yesha Zheng[‡], Hortense Mazon[§], Elena Milgrom[¶], Norton Kitagawa[‡¶], Erik Kish-Trier[¶], Albert J. R. Heck[§2], Patricia M. Kane[¶], and Stephan Wilkens[‡3]

From the [‡]Department of Biochemistry, University of California, Riverside, California 92521, the [§]Biomolecular Mass Spectrometry and Proteomics Group, Bijvoet Center for Biomolecular Research and Utrecht Institute for Pharmaceutical Sciences, Utrecht University, 3584 CA Utrecht, The Netherlands, and the [¶]Department of Biochemistry & Molecular Biology, SUNY Upstate Medical University, Syracuse, New York 13210

The subunit architecture of the yeast vacuolar ATPase (V-ATPase) was analyzed by single particle transmission electron microscopy and electrospray ionization (ESI) tandem mass spectrometry. A three-dimensional model of the intact V-ATPase was calculated from two-dimensional projections of the complex at a resolution of 25 Å. Images of yeast V-ATPase decorated with monoclonal antibodies against subunits A, E, and G position subunit A within the pseudo-hexagonal arrangement in the V_1, the N terminus of subunit G in the V_1-V_0 interface, and the C terminus of subunit E at the top of the V_1 domain. ESI tandem mass spectrometry of yeast V_1-ATPase showed that subunits E and G are most easily lost in collision-induced dissociation, consistent with a peripheral location of the subunits. An atomic model of the yeast V-ATPase was generated by fitting of the available x-ray crystal structures into the electron microscopy-derived electron density map. The resulting atomic model of the yeast vacuolar ATPase serves as a framework to help understand the role the peripheral stalk subunits are playing in the regulation of the ATP hydrolysis driven proton pumping activity of the vacuolar ATPase.

Vacuolar ATPases (V-ATPases; V_1V_0-ATPases)[4] are ATP hydrolysis driven proton pumps found in the endomembrane system of eukaryotic organisms where their proton pumping action is involved in vital cellular processes including protein trafficking, receptor-mediated endocytosis, and neurotransmitter release (1–3). In higher organisms, V-ATPases are also found in the plasma membrane of specialized cells such as renal intercalated cells or bone osteoclasts. Here, the enzyme pumps protons across the plasma membrane to the space outside of the cell, thereby functioning for example, in urine acidification and bone remodeling (4). Due to its involvement in so many essential cellular processes, it is not surprising that defects in the human vacuolar ATPase play a direct role in a variety of widespread diseases such as osteopetrosis (5), osteoporosis (6), gastritis (6), diabetes (7), renal tubular acidosis (8), sensorineural deafness (9), cancer (10), and AIDS (11).

The vacuolar ATPase is a large, membrane-bound multisubunit enzyme complex composed of two functional domains: a water soluble V_1 and a membrane-embedded V_0. The two domains are joined by a stalk domain, which acts as a conduit to couple catalytic events taking place on the V_1 to ion translocation across the membrane-embedded V_0. The yeast V-ATPase contains 14 different subunits with relative molecular masses ranging from 9,000 to 100,000. Eight different subunits A, B, (C), D, E, F, G, and H make up the V_1 domain and the V_0 contains the remaining six subunits that are called *a*, *c*, *c′*, *c″*, *d*, and *e*. Subunit *e*, originally described for the bovine and insect enzyme (12–13) has only recently been found to be a subunit of the yeast complex (14), suggesting that this subunit is a component of all eukaryotic V-ATPase membrane domains. The copy number of the subunits in the yeast V-ATPase complex is $A_3B_3(C)DE_3FG_3H$ for the V_1 and $a(c,c')_{4-5}c''de$ for the V_0.

The vacuolar ATPase is evolutionary related to the F-ATPase and it has been shown that both enzymes employ a rotary mechanism of ATP hydrolysis coupled to proton translocation (15). According to the current model of V-ATPase function, hydrolysis of ATP taking place at the interface of the A and B subunits of the V_1 drives rotation of the central stalk (rotor) composed of subunits D, F, *d*, and the ring of proteolipid subunits *c*, *c′*, and *c″* (16–18). Peripheral stalks composed of subunits E, G, H, and C connect the N-terminal domain of the V_0 *a* subunit with the catalytic A_3B_3 domain. Proton translocation takes place at the interface of the C-terminal domain of the *a* subunit and the rotating proteolipid ring. A major difference between F- and V-ATPase is that the activity of the latter is controlled by a unique mechanism of regulation to adapt to the nutritional or developmental status of the organism (19–20). In yeast, it has been shown that V-ATPase reversibly dissociates into V_1 and V_0 in response to glucose withdrawal, and restoration of glucose induces efficient re-assembly of the V-ATPase from the existing pool of V_1 and V_0 domains.

Electron microscopy has provided some knowledge about the overall structure of V-ATPases from bovine (21–23), insect

* This work was supported, in whole or in part, by National Institutes of Health Grants GM58600 and CA100246 (to S. W.) and GM50322 (to P. M. K.). The costs of publication of this article were defrayed in part by the payment of page charges. This article must therefore be hereby marked "*advertisement*" in accordance with 18 U.S.C. Section 1734 solely to indicate this fact.

[S] The on-line version of this article (available at http://www.jbc.org) contains supplemental Figs. S1–S4 and Tables S1 and S2.

[1] Present address: Key Laboratory of Industrial Biotechnology, Ministry of Education, School of Biotechnology, Jiangnan University, 1800 Lihu Ave., Wuxi 214122, China.

[2] Supported by the Netherlands Proteomics Centre and the Netherlands Research Council for Chemical Sciences.

[3] To whom correspondence should be addressed: Dept. of Biochemistry and Molecular Biology, SUNY Upstate Medical University, Syracuse, NY 13210. Tel.: 315-464-8703; Fax: 315-464-8750; E-mail: wilkenss@upstate.edu.

[4] The abbreviations used are: V_1V_0, proton pumping vacuolar ATPase; V_1, water soluble domain of the vacuolar proton pumping ATPase; V_0, membrane bound domain of the proton pumping vacuolar ATPase; EM, electron microscopy; MS, mass spectrometry; ESI, electrospray ionization; HA, hemagglutinin; PDB, Protein Data Bank.

(24–26), plants (27, 28), fungi (29), and yeast (Refs. 30 and 31, reviewed in Ref. 32), but the detailed arrangement of the subunits in the complex, especially in the stalk region, remains a matter of ongoing controversy. Previously, we have determined the binding sites of subunits H (23) and C (31) in the V-ATPase stalk region and we have argued that these two subunits are positioned to play a key role in the mechanism of reversible dissociation and activity silencing, respectively (32).

Here we report the three-dimensional structure of the vacuolar ATPase from the yeast *Saccharomyces cerevisiae* calculated from electron microscopic images at a resolution of 25 Å. Antibody labeling was used to localize subunits A, E, and G. Electrospray ionization tandem mass spectrometry of intact yeast V_1-ATPase revealed that subunits E and G are most easily lost during collision-induced dissociation, consistent with a peripheral binding location of these two subunits. This information together with our recent localization of subunits C and H and the published x-ray crystal structures of V- and F-ATPase subunits and domains allowed us to construct a detailed structural model of the yeast vacuolar ATPase. We speculate that the C subunit is interacting with two peripheral stalks and that breaking or forming these interactions is a key step in the mechanism of reversible V-ATPase dissociation/re-association.

EXPERIMENTAL PROCEDURES

Materials—All chemicals were from Sigma unless noted otherwise. Premixed YEPD (1% yeast extract, 2% peptone, 2% glucose) and leucine dropout medium were from Difco and Invitrogen, respectively. M2 anti-FLAG affinity-agarose, anti-FLAG IgG, and FLAG peptide anti-HA IgG were from Sigma. Anti-subunit A and B monoclonal antibodies were from Molecular Probes, Inc. Protein concentrations were determined with the BCA assay system (Pierce).

Yeast Strains and Culture Conditions—The yeast strains expressing Vma10p fused to a N-terminal FLAG tag and Vma4p fused to a C-terminal triple HA tag were described earlier (30, 33).

Preparation of Yeast V_1- and V_1V_0-ATPase—Yeast V_1-ATPase with a FLAG tag fused to the N terminus of subunit G (Vma10p-FLAG) was purified as described (30). Intact yeast V_1V_0-ATPase (Vma10p-NT-FLAG) was purified as described (31) with the following modification. Briefly, vacuoles were extracted at a protein concentration of 1 mg/ml with 1% dodecyl maltoside and the extracted protein was subjected to glycerol density gradient centrifugation in the presence of 0.05% P-MAL C12 (Anatrace). Prior to use, the P-MAL C12 was subjected to ultrafiltration through a 10-kDa cut-off Amicon Ultra centrifugation filter device to remove the larger polymers. V-ATPase containing fractions were concentrated by ultrafiltration and used for antibody labeling experiments (see below). Purified yeast V-ATPase containing a HA tag fused to the N terminus of subunit C (Vma5p-HA; characterized in Ref. 34) was a kind gift from Dr. Michael Forgac, Tufts University School of Medicine, Boston, MA. Initial image analysis of the Vma5p-HA V-ATPase has been described (31).

Electrospray Ionization Tandem Mass Spectrometry—The V_1-ATPase sample was subjected to buffer exchange into 100 mM ammonium acetate, pH 6.8, by using an Ultrafree-0.5 centrifugal filter device with a cut-off of 10 kDa (Millipore). The sample was sprayed from a solution of 2 μl containing 0.5 μM (0.3 mg/ml) of the complex. The native and tandem mass spectrometry measurements were performed in positive ion mode on a modified Q-TOF (quadrupole time-of-flight) instrument (Micromass, UK) (35, 36). Nanospray glass capillaries were used to introduce the samples into the Z-spray source. The source pressure was increased to 10 mbar to create increased collisional cooling. The needle voltage was 1,500 V, and the sample cone voltage was 150 V. For the tandem mass spectrometry (MS/MS) measurements, precursor ions of specific m/z were selected in the quadrupole. Subsequently, they were accelerated before the collision cell applying voltages from 10 to 200 V over this cell. Xenon was used as the collision gas in the MS/MS experiments to increase ion transmission and energy transfer efficiency during the process (37).

Preparation of Anti-subunit A Fab—Anti-subunit A monoclonal antibody (mouse IgG2a 8B1) was digested by immobilized papain (Pierce) according to the manufacturer's protocol. The progress of monoclonal antibody digestion was followed by SDS-PAGE. Fab fragments were used without further purification.

Immunolabeling—For immunolabeling, V-ATPase containing the targeted antigen was mixed with the corresponding antibody at a defined molar ratio and incubated at 4 °C for 1 h. V_1-ATPase was mixed with 8B1 Fab at a 1:6 molar ratio. For detection of subunits E and G, Vma4p-CT-HA and Vma10p-NT-FLAG V-ATPase were incubated with antibody and the unbound antibody was separated from labeled V-ATPase by glycerol density centrifugation in the presence of 0.05% dodecyl maltoside as described in Ref. 31. V-ATPase containing fractions were concentrated by ultrafiltration for analysis by SDS-PAGE or used directly for negative stain electron microscopy.

Negative Stain Electron Microscopy—For negative staining, 5 μl of protein solution at a concentration of between 20 and 50 μg/ml in Tris-buffered saline (20 mM Tris-Cl, pH 7.2, 150 mM NaCl) was applied to glow discharged carbon-coated copper grids. Grids were washed once with water, stained with 1% uranyl acetate for 1 min, and air-dried. Grids were examined in a Tecnai 12 transmission electron microscope operating at 100 kV. Images were recorded in low dose mode with a 2048 × 2048 pixel charge-coupled device (Ultrascan 1000, Gatan Inc.) in single frame or 2X2 montage mode. Images of stained samples were recorded with an underfocus of ~1 μm and an electron optical magnification setting of ×26,500, placing the 1st zero of the contrast transfer function at around 1/20 $Å^{-1}$. Images of anti-HA antibody-labeled Vma4p-CT-HA V-ATPase were recorded with a JEM-2100 (JEOL) transmission electron microscope operating at 200 kV. Images were recorded with a F224HD CCD camera (TVIPS) at an electron optical magnification of ×40,000 and an underfocus of 1500 nm. Pixel sizes on the specimen level were determined with bacteriorhodopsin and catalase two-dimensional crystals as standards.

Image Analysis and Three-dimensional Reconstruction—Images were analyzed with the EMAN (38) and IMAGIC 5 (39) software packages running on Macintosh G5 and SGI workstations (O2 and Octane) essentially as described (21–23, 30, 31).

Single particles were selected interactively from CCD frames using the Boxer program in the EMAN package (38). All subsequent image analysis was performed with the IMAGIC5 package of programs (39). The images were normalized and band pass filtered to remove low (<0.008 $Å^{-1}$) and high (>0.133 $Å^{-1}$) spatial frequencies. The data sets were then analyzed by the alignment by classification procedure (40) leading to sets of initial references that were used in a first multireference alignment step. The multireference alignment was iterated until no further improvement in the class sums was obtained.

Three-dimensional Reconstruction—To start up the yeast V-ATPase three-dimensional reconstruction, projections of the three-dimensional model of the bovine V-ATPase (23) were used as references to align a data set of ~25,000 images of yeast V-ATPase (Vma5p-HA) (31). After seven rounds of refinement, the resulting model was filtered to remove noise (density not connected to the main volume of the model) and forward-projected along 49 directions uniformly distributed over the Euler sphere. The 49 projections were normalized and used as references in a new multireference alignment step. Two hundred images aligned to each reference were averaged and used as input projections for a new three-dimensional model. This process was iterated increasing the numbers of forward projections and images averaged for each reference until no further improvement was observed. At this point, classification of the aligned data set produced very similar class sums compared with the ones used to start up the three-dimensional reconstruction (not shown). The resolution of the final reconstruction was estimated by calculating the Fourier shell correlation between two three-dimensional models each calculated from half the input projections as described in Ref. 41. The final model was filtered to 0.05 $Å^{-1}$, corresponding to the first zero in the contrast transfer function.

Fitting of Atomic Structures of Subunits—The atomic structures we used to fit into the V-ATPase model were the crystal structure of the $\alpha_3\beta_3$ subcomplex of ATP synthase from *Bacillus* PS3 (Protein Data Bank 1sky), the crystal structure of subunit C of the yeast V-ATPase (PDB 1u7l; and the low resolution conformer, Ref. 42, coordinates kindly provided by Dr. Nathan Nelson, Tel Aviv University, Tel Aviv, Israel), the crystal structure of the γ subunit of bovine mitochondrial F_1-ATPase (PDB 1e79), the crystal structure of subunit H of the yeast V-ATPase (PDB 1ho8; Ref. 43), the ac_{12} subcomplex of *Escherichia coli* ATP synthase derived from NMR data and modeling (PDB 1c17) and the k_{10} ring of the A/V-ATPase from *Enterococcus hirae* (PDB 2bl2). The following structures were used as templates for homology modeling using Fugue and SwissModel: the crystal structure of the A subunit of the archaeal A-ATPase from *P. horikoshii* (PDB 1vdz), the crystal structure of the B subunit of the A-ATPase from *Methanosarcina mazei* (PDB 2c61), and the crystal structure of subunit C (the homolog of yeast V-ATPase subunit d) of V-ATPase from *Thermus thermophilus* (PDB 1r5z). The structural model of the subunit EG heterodimer (peripheral stalk) included the crystal structure of the C-terminal domain of subunit E from *Pyrococcus horikoshii* (PDB 2dma). The N-terminal domains of the EG heterodimer were modeled as a pair of interacting α helices based on secondary structure and coiled coil prediction (44). Automated, semi-automated, and manual docking was done with Situs (45) and Chimera (46), respectively. A description of the fitting procedures and the rationales for placing the subunits is given in supplementary information Table S2.

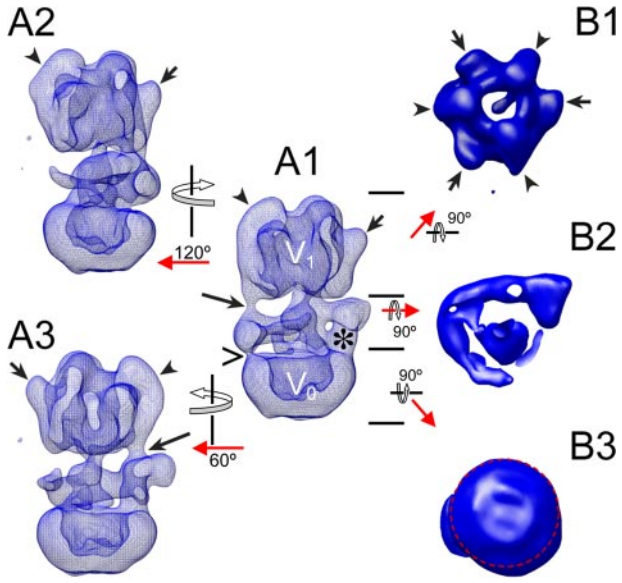

FIGURE 1. **Three-dimensional structural model of the yeast vacuolar ATPase.** The model was calculated from a data set of 25,000 single images at ~25 Å resolution. The *short arrows* and *arrowheads* point to the elongated- and knob-like densities at the top of the V_1. The *long arrows* point to the peripheral stalks resolved in the three-dimensional model. The > sign points to a thin connection between subunit C and the membrane domain (see below for a discussion on the binding position of subunit C). The *asterisk* indicates the location of the N-terminal domain of subunit *a* (a_{nt}). The short *arrows* and *arrowheads* in B1 point to the alternating A and B subunits in the V_1, respectively. The image in *B2* shows the arc-like arrangement of the peripheral stalk proteins surrounding the central stalk. The image in *B3* shows the bottom view of the V_0. The asymmetry of the V_0 is indicated by the *red circle*. For details, see text.

RESULTS

Yeast V-ATPase Three-dimensional Model—Fig. 1 shows surface representations of the three-dimensional EM-derived model of the yeast vacuolar ATPase. The volume was reconstructed from 220 averages obtained from a data set of ~25,000 molecular images. The resolution of the final model was 25 Å as determined by the Fourier shell correlation algorithm using a cut-off of 0.5 (see supplemental Fig. S1). Image analysis was initiated by a first round of multireference alignment using projections of the three-dimensional model of the bovine V-ATPase (23). All subsequent refinements were performed independently of the bovine model (a comparison of the yeast and bovine V-ATPase models is shown in supplemental Fig. S2). Overall, the complex has a cylinder-like shape with a diameter of about 13.9 nm and a height of about 24.5 nm. The cytoplasmic V_1 domain (see Fig. 1, *A1*, for the assignment of the V_1 and V_0 domains) has a pseudo 3-fold symmetry as evident from the top view shown in image *B1* (see *arrows* and *arrowheads*). The pseudo 3-fold symmetry of the V_1 is due to the alternating arrangement of the three A and B subunits. Three of the large subunits show the earlier described "knob"-like densities (Ref. 21, see *short arrows* in images *A1–A3* and *B1*). The other three subunits have elongated densities bound at their periphery (see *arrowheads*). The membrane-embedded V_0 has a smooth sur-

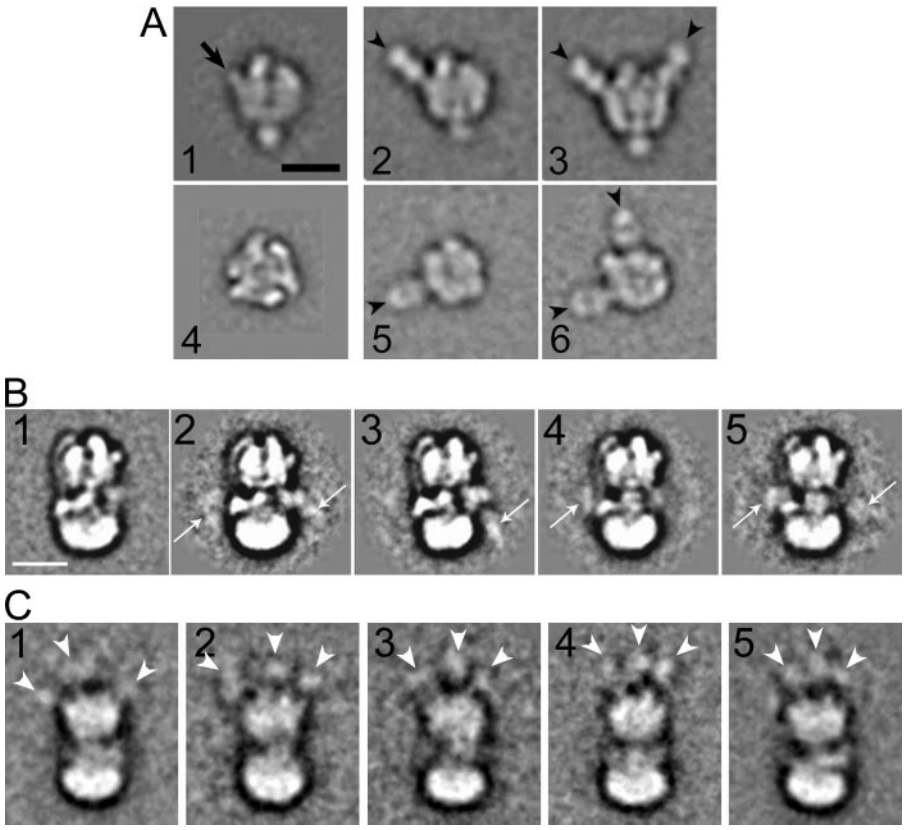

FIGURE 2. **Immunolocalization of subunits A, G, and E yeast V-ATPase.** *A*, image analysis of V_1-ATPase labeled with anti-A Fab. Images *1* and *4* show top and side view of unlabeled V_1 (30). Images *2* and *3* show side views and *5* and *6* top views of anti-A Fab-labeled V_1. Averages were obtained that showed either one (images *2* and *5*) or two Fabs bound. No averages with three Fab bound were seen in this analysis, possibly due to steric hindrance of the third antibody binding site. Images *2* and *3* are from Ref. 32. Averages 1–6 were calculated from ~200 single molecule images each. *B*, yeast V-ATPase containing a FLAG tag fused to the N terminus of subunit G was labeled with anti-FLAG monoclonal antibody. Averages (~250 images each) show additional density due to the IgG either on one side (see *arrows* in images *3* and *4*) or on both sides (images *2* and *5*). *C*, V-ATPase containing three HA tags fused to the C terminus of subunit E was labeled with anti-HA monoclonal antibody. Despite the overall lower quality of the averages (100–150 images each), three additional densities can be seen at the top of the V_1 domain. For details, see text. *Bars* = 10 nm.

face without obvious protrusions. The bottom view of the V_0, however, shows a significant asymmetry due to the presence of the C-terminal domain of the single copy V_0-*a* subunit at the outside of the proteolipid ring (see *red circle* in image *B3*). The V_1 and V_0 domains are joined by a collar-like structure that surrounds the central stalk in an arc-like fashion for about 270° (see image *B2*). The arc is connected to the V_1 by two clearly resolved densities (peripheral stalks; see *long arrows* in images *A1* and *A3*). These two peripheral stalks extend from the elongated densities running down from the top of the V_1 domain. An elongated density can also be seen at the peripheral top half of the third subunit of that kind (see *arrowhead* in image *A2*), this third elongated density is less well resolved and does not seem to extend into a peripheral stalk at the contour level chosen to render the volumes (see Fig. S3 for a map at lower contour showing the third peripheral stalk density more clearly). The arc surrounding the central stalk is connected to the membrane-embedded V_0 by the N-terminal domain of the V_0-*a* subunit (see *asterisk* in image *a*1). Another weak connection is seen on the opposite side (see *open arrow*).

Immunolocalization of Subunits: Subunit A—The catalytic core of the V-ATPase is made of three subunit AB heterodimers that are arranged in a pseudo-hexagonal fashion around a central cavity. Both A and B subunits bind nucleotide, but only the A subunits catalyze the hydrolysis reaction. To determine which of the large densities in the V_1 domain correspond to subunit A, purified yeast V_1-ATPase was incubated with Fab fragments derived from subunit A-specific 8B1 monoclonal antibody at a molar ratio of 1:6. Fig. 2*A* shows image analysis of anti-subunit A-labeled V_1 ATPase. A data set of 7000 single particles was analyzed by alignment and classification. Fig. 2*A*, images 1 and 4 show a side and top view projection of unlabeled V_1-ATPase, respectively (32). Images 2, 3, 5, and 6 of Fig. 2*A* show four of the most representative averages of V_1-ATPase labeled with the 8B1 Fab. The comparison with unlabeled V_1-ATPase (images 1 and 4) revealed that the Fab binds to the knob-like densities at the top of V_1-ATPase (see *arrow* in image 1 of Fig. 2*A*), confirming our earlier speculation (21) that the three knob-like structures are part of the three A subunits (see *arrowheads*). As seen in the class averages, up to two copies of Fab can be seen bound to one V_1 molecule. It is possible that a third Fab was hidden in projection, but the possibility that the three A subunits exist in different conformations and that one of them was unable to bind the Fab cannot be excluded at this point.

Immunolocalization of Subunits E and G—Purified yeast V-ATPase containing subunit G tagged with a FLAG peptide at the N terminus was mixed with anti-FLAG monoclonal antibody at a molar ratio of 1:5 and excess antibody was separated from labeled V-ATPase by density gradient centrifugation. SDS-PAGE of gradient fractions showed that anti-FLAG antibody was co-migrating with the V-ATPase peak during the centrifugation indicating binding of the antibody to the G-subunit N terminus in the native complex (SDS-PAGE not shown). A data set of ~14,600 single particles were selected from electron micrographs and representative class sums obtained after several rounds of alignment and classification are shown in Fig. 2*B*, *images 2–5*. For comparison, an average of unlabeled V-ATPase is shown in *image 1* in Fig. 2*B*. Additional densities can be seen near the V_1-V_0 interface (see *arrows* in *images 2–5*). The signal of antibody appears somewhat weaker compared with the anti-A Fab, probably due to the flexibility of the FLAG peptide attached to the subunit G N terminus. Some averages show the antibody near the density assigned as subunit C (31) (*image 4*),

whereas in other averages, additional density is visible in the region where subunit H and the N-terminal domain of subunit *a* is located (23) (image *3*). In a small number of averages, additional density can be seen on both sides of the complex (*images 2* and *5*). These results indicate that the N terminus of subunit G is located in the interface between V_1 and V_0 and that at least two of the three copies of the subunit are on different sides of the complex.

For the localization of subunit E, purified yeast V-ATPase containing subunit E tagged with a triple HA antigen at the C terminus was mixed with anti-HA monoclonal antibody at a molar ratio of 1:10, and excess antibody was separated from labeled V-ATPase by density gradient centrifugation. In this experiment, essentially all the added antibodies co-migrated with the V-ATPase as determined by SDS-PAGE of the gradient fractions (not shown). This might be explained by the fact that subunit E contained three consecutive HA tags and that there are three copies of the subunit in the complex. The peak fraction of the density gradient containing anti-HA antibody labeled V-ATPase was analyzed by negative stain electron microscopy and image analysis. The results are summarized in Fig. 2*C*. As can be seen, the overall quality of the averages of anti-HA-labeled V-ATPase projections is somewhat lower compared with the images of anti-G-labeled V-ATPase shown in Fig. 2*B*. The lower quality of the anti-HA-labeled V-ATPase projection averages might be explained by the fact that the three (or more) anti-HA IgGs bound to the complex lead to some interference with the alignment of the typical V-ATPase features. Nevertheless, additional density due to the anti-HA antibodies can be seen at the top of the V_1 domain in the anti-HA-labeled molecules (compare with the projection of unlabeled V-ATPase shown in Fig. 2*B*, *image 1*). The presence of additional density connected to three locations at the top of the V_1 (see *arrowheads* in images C1–5) is consistent with three copies of subunit E as previously reported (47). Taken together, the subunit G and E labeling experiments reveal the orientation of both subunits, with the N termini near the V_1-V_0 interface and the C termini at the top of the V_1 domain.

Tandem Macromolecular Mass Spectrometry on Intact V_1-ATPase—Previously, we have analyzed V_1-ATPase purified from yeast via affinity chromatography by electrospray ionization mass spectrometry (47). The spectra revealed three species (complexes I, II, and III), the most abundant one (complex I, ~57–72%) having a molecular mass of 593,000 kDa, with two minor species at 553,000 kDa (complex II, ~12–17%) and 428,000 kDa (complex III, ~16–25%) (Fig. 3*A*). The high accuracy of the mass measurement allowed unambiguous determination of the subunit stoichiometry of the three V_1-ATPase species, indicating that the most abundant species contained three E and three G subunits each (47). Here, we used tandem mass spectrometry as a tool to further analyze the arrangement of the stalk subunits in the V_1-ATPase from yeast. In such experiments, mass-selected ions of the complex are activated by collisional excitation inside the collision cell of the mass spectrometer. This activation is fine tuned to lead to a gas-phase decomposition of the multisubunit complex, typically resulting in elimination of subunits that are more loosely attached at the surface of the protein complex (48, 49). First, we mass-selected the 52+ charge state ion of the 593-kDa complex at an *m*/*z* value of 11,450 in the quadrupole analyzer and accelerated them into the gas-filled collision cell. At relatively low collision voltage (100 V) (Fig. 3, *B–D*), only subunits E and G were eliminated from the complex. This resulted in the concomitant formation of ions without subunit E in the high *m*/*z* region (which had the most abundant charge state distribution), as well as ions without subunit G (Fig. 3*D*). The masses of the different species are summarized in supplemental Table S1. At a collision voltage of 100 V the 52+ parent ion represented still the most abundant signal in the tandem mass spectrum. Upon increasing the acceleration voltage to 200 V (Fig. 3, *E–G*), we observed the subsequent dissociation of a second subunit E or G. Therefore, again concomitantly in the high *m*/*z* region we detected ions originating from complex I without two subunits E, which was the most abundant species, and the complex without one subunit E and one subunit G (Fig. 3*G*). Moreover, at this higher collision voltage subunit H was ejected from complex I resulting in the simultaneous formation of ions originating from the complex I without subunit H. At 200 V the 52+ precursor ion had vanished nearly completely from the tandem mass spectra. We also performed tandem mass spectrometry on the isolated 43+ charge state ion of the 428-kDa complex III at an *m*/*z* value of 9,960 and also for this complex, subcomplexes lacking subunit E were most abundant (not shown, for the measured masses see supplemental Table S1).

Thus, the mass spectrometry analysis by gas-phase dissociation revealed that subunits E and G are preferentially eliminated from the A_3B_3 (or A_2B_2) complexes, consistent with these two subunits being located at the outer surface of the V_1 where they might be bound via relatively weak interactions with the core of the ATPase domain. Interestingly, the most abundant species were subcomplexes from which subunit E was lost while subunit G stayed bound. The preferential loss of subunit E suggests that at least part of the binding energy between the EG peripheral stators and the A_3B_3 catalytic domain is mediated by subunit G because if the interaction of subunit G with the V_1-ATPase complex were only via subunit E, then any loss of subunit E would lead to a concomitant loss of subunit G. Subunit H on the other hand required a collision voltage of 200 V for dissociation, indicating that its affinity for the catalytic core is slightly higher compared with the EG heterodimer.

As discussed in Ref. 47, we do not know at this point whether the appearance of complexes II ($A_3B_3DE_2FG_2H$) and III ($A_2B_2DE_2FG_2H$) is due to electrospray ionization or whether these subcomplexes are already present in the preparation injected into the mass spectrometer. Support for the latter possibility comes from the fact that only trace amounts of individual subunits (only E and G) were seen in the low *m*/*z* range in the native mass spectra of the yeast V_1-ATPase preparation (47). It is possible that complexes II and III are already present in the yeast cytoplasm (assembly intermediates) but we cannot rule out at this point that at least some of the subcomplexes were formed during protein purification and/or sample preparation for mass spectrometry (*e.g.* exchange of the protein into mass spectrometry compatible buffer). Note, however, that no loss of A and/or B subunits occurs under the conditions used for collision-induced dissociation (100/200 V acceleration

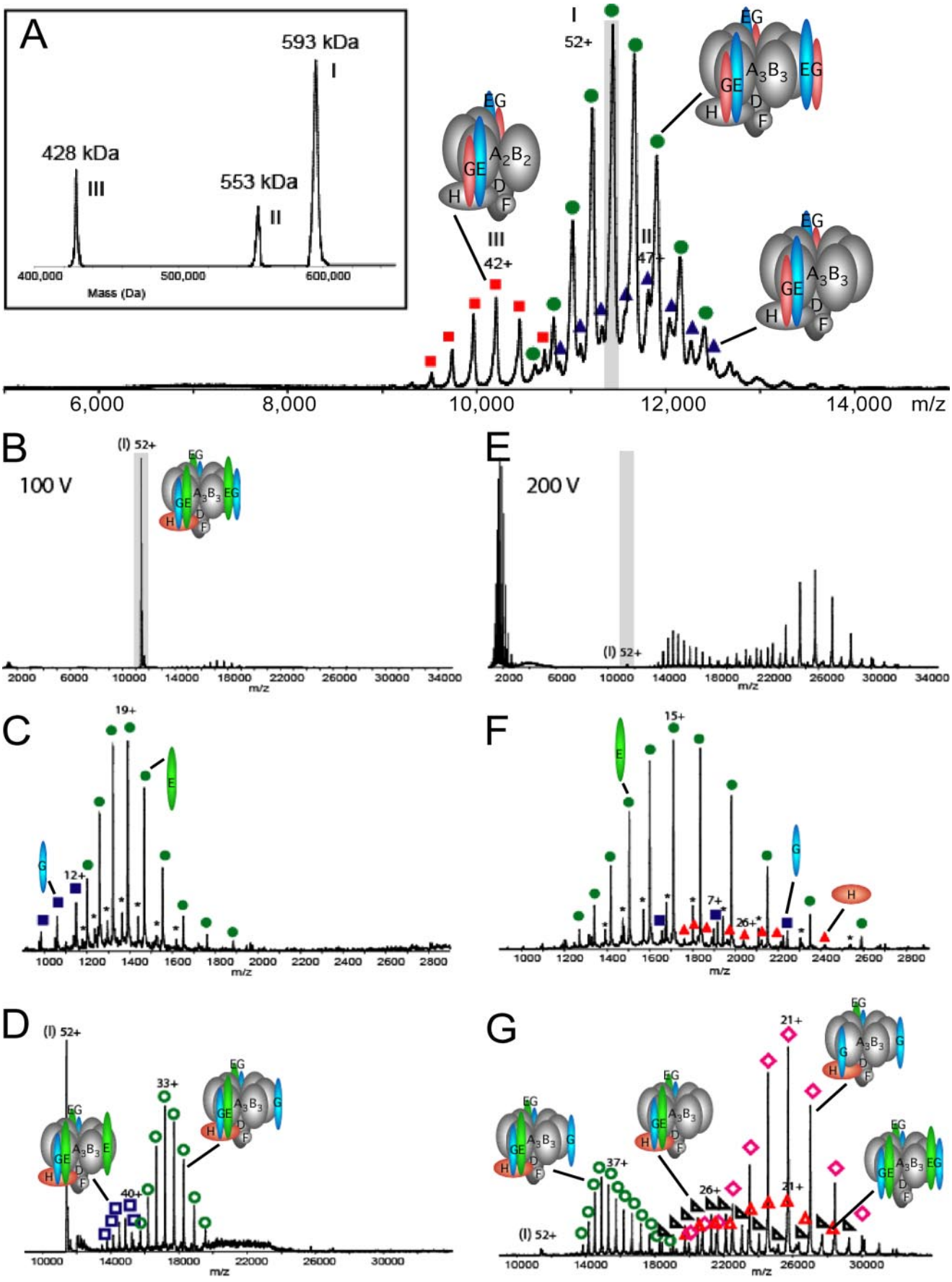
A
593 kDa
I
428 kDa
III
553 kDa
II
400,000
500,000
600,000
Mass (Da)
I
52+
III
42+
II
47+
6,000
8,000
10,000
12,000
14,000
m/z
B
100 V
(I) 52+
C
19+
12+
D
(I) 52+
33+
40+
E
200 V
(I) 52+
F
15+
7+
26+
G
21+
37+
26+
21+
(I) 52+

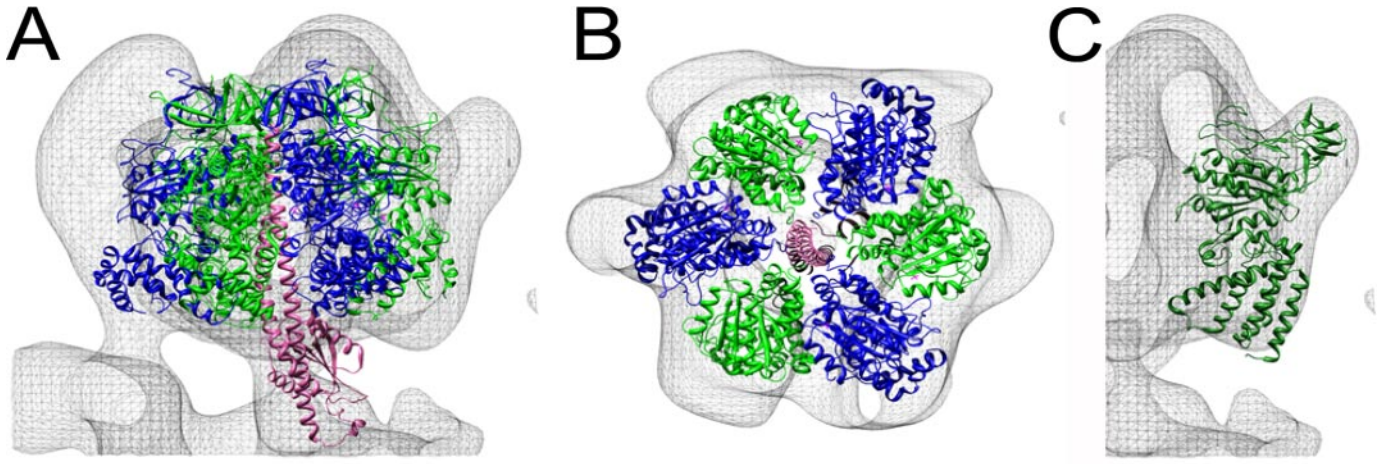

FIGURE 4. **Fitting of F_1-ATPase $\alpha_3\beta_3$ catalytic domain, central rotor, and A-ATPase A subunit into the yeast V-ATPase three-dimensional model.** *A*, side view, and *B*, top view of the resulting fit. The subunits are α (*blue*), β (*green*), and γ (*pink*). *C*, manual fitting of the partial structure of the A-ATPase subunit A (PDB 1vdc) into the yeast V-ATPase model. For details of the fitting procedure, see "Experimental Procedures" and supplemental Table S2.

potential), indicating that A_3B_3DF represents a relatively stable core complex of the V_1-ATPase.

Fitting of Atomic Resolution Structures of Subunits into the Three-dimensional Model—Automated, semi-automated, and manual fitting of available crystal structures was done with Situs (45) and Chimera (46). The fitting procedures and the rationale for the placement of the subunits are summarized in supplementary information Table S2.

The A_3B_3 Catalytic Domain—To verify the absolute handedness of the yeast V-ATPase three-dimensional model, we generated a mirror version of the model and used automated docking to fit the $\alpha_3\beta_3$ catalytic domain of the structurally related F_1-ATPase (1sky) into both models. The best fit of the $\alpha_3\beta_3$ subcomplex was obtained with the model as shown in Fig. 1, indicating that the final model of the complex has the correct handedness. Fitting of the F-ATPase $\alpha_3\beta_3$ hexamer is shown in Fig. 4, *A* and *B*. In the orientation generated by automated fitting, the α and β subunits take the positions of the V_1 B and A subunits, respectively, again consistent with the earlier assignment based on the anti-A subunit immunolabeling (Fig. 2*A*). Fig. 4*C* shows fitting of the crystal structure of the A subunit of the related archaeal A-ATPase (PDB 1vdz) into the EM density corresponding to yeast V-ATPase subunit A. As can be seen, the globular structure representing the non-homologous region in the primary sequence of the A-ATPase A-subunit fits well into the knob-like densities at the top periphery of the V_1-domain. Note that the N-terminal domain in the A-ATPase A subunit was not resolved in the crystal structure of the isolated subunit (50). Next, the atomic structure of the F_1-γ subunit (PDB 1e79) was manually placed into the central stalk density (Fig. 4*A*). The criteria used for fitting was to maximize the overlap between the crystal structure and EM-derived electron density. In the fit obtained this way, the bottom of the F-ATPase γ subunit makes contact with the density located in the opening of the proteolipid ring that we had assigned earlier as subunit *d* (see below) (22, 32).

Peripheral Stalks—Currently, there is no atomic resolution structure available for the intact peripheral stalk (subunit EG heterodimer) of the eukaryotic or bacterial V-ATPase or the related A-ATPase. A crystal structure of the C-terminal domain of the E subunit of the A-ATPase from *P. horikoshii* has been reported (51). In the structure, the C-terminal domain of subunit E forms a tight dimer but as we have shown earlier, adding the second stalk forming subunit (subunit G is called subunit H in the A-ATPase, not to be confused with subunit H, Vma13p, in the yeast V-ATPase), leads to formation of a monodisperse subunit EH heterodimer with 1:1 stoichiometry (44). A similar 1:1 EG heterodimer was also reported earlier for the yeast V-ATPase (52). Based on the available structure of the subunit E C-terminal domain (51), the EM analysis of the yeast EG complex (52) and secondary structure prediction (44), we have modeled the yeast EG heterodimer as shown in Fig. 5*A*. There is evidence that part of the EG heterodimer (as well as the related EH heterodimer from the A-ATPase) is folded as a coiled coil. To which extent the subunits exist in a coiled coil, which part is involved, and whether it is of left- or right-handed nature is not known at this point. We have therefore represented the N-terminal domains of E and G as parallel α helices. Next, we fitted the EG heterodimer into the elongated densities visible at the periphery of the B subunits (see *arrowheads* in Fig. 1). Although the electron density of the model is well resolved for the peripheral stalk visible on the *left* in Fig. 5*B* (EG^1), the connecting density for the stalk on the *right* (EG^2) is not visible at the contour level chosen to render the model (see *arrow* in

FIGURE 3. **Tandem mass spectrometry of yeast V_1-ATPase.** *A*, electrospray ionization mass spectrometry spectrum of intact V_1-ATPase (taken from Ref. 47) showing three species. The *52*+ charge state of the most abundant complex (593 kDa; *I*), which has the stoichiometry $A_3B_3DE_3FG_3H$ was selected for collisional activation, highlighted in *gray*. *B–G*, tandem mass spectra of V_1-ATPase sprayed from aqueous 100 mM ammonium acetate, pH 6.8. Dissociation of the 52+ ion of the 593-kDa V_1-ATPase complex at a collision voltage of 100 V (*B*) with zoom in the *m/z* regions 900–2,900 (*C*) and 9,000–34,000 (*D*). Dissociation of the 52+ ion of the complex at a collision voltage of 200 V (*E*) with zoom in the *m/z* regions 900–2,900 (*F*) and 9,000–34,000 (*G*). The dissociated subunits E, G, and H are represented by *green circle*, *blue square*, and *red triangle*, respectively. The product ions of five different complexes are indicated by the *empty green circle* (loss of one subunit E), *empty pink rhombus* (loss of two subunits E), *empty blue square* (loss of one subunit G), *empty black triangle* (loss of one subunit G and one subunit E), and *empty red triangle* (loss of one subunit H). The charge series marked with a *asterisk* corresponds to a degraded form of subunit E.

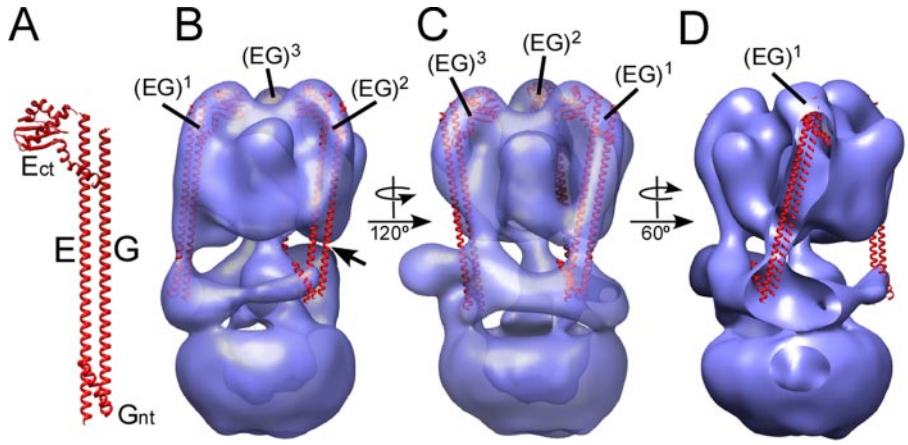

FIGURE 5. **Fitting of the EG structural model into the yeast V-ATPase three-dimensional model.** *A*, structural model of the EG heterodimer. The model is based on the crystal structure of the C-terminal domain of the A-ATPase E subunit (E_{ct}; PDB 2dma) as well as secondary structure and coiled coil prediction (44). *B* and *C*, fitting of the three copies of the EG heterodimer into the V-ATPase three-dimensional model. *D*, in this orientation, part of the density is cut away to allow a view inside the three-dimensional model. As can be seen, the stators connect the B subunits and the collar domain at an angle (most pronounced for stator EG^1 where the angle is ~20°).

panel B, for a lower contour representation of the model, see supplemental Fig. S3). Turning the model 120° reveals the third stator on the left side of the model as shown in *panel C* (EG^3). Placement of the third stator is slightly to the left of the connecting density, which we think is formed at least in part by the interaction between subunit H (Vma13p; not to be confused with subunit H in the A-ATPase) and subunit B (see below). As can be seen, the fits suggest that the peripheral stalks are not parallel to the long axis of the complex but rather at an angle of about 20°. This is most clearly seen in Fig. 5*D*, which shows stator 1 (EG^1) within the electron density of the model.

Subunit C—Previously, we have mapped subunit C (Vma5p) in the yeast V-ATPase using immunoelectron microscopy (31). According to the data, subunit C binds in the V_1-V_0 interface, wrapping around the central rotor domain, across from where subunit H is bound (23). Consistent with the two-dimensional projections (31), the crystal structure of Vma5p was placed into the V-ATPase electron density via manual docking. Fig. 6*A* shows an overlay of the crystal structures of both conformers of subunit C (42). As can be seen, whereas the "foot" domains match very well, the "head" domains have a different orientation (the high resolution conformer is in *green* and the low resolution conformer in *yellow*). Fig. 6, *B* and *C*, shows fitting of both conformers into the yeast V-ATPase model. As can be seen, the lower resolution conformer provides a better fit into the EM-derived electron density compared with the high-resolution structure. Furthermore, it can be seen that the placement of subunit C as seen in Fig. 6, *B* and *C*, brings both foot and head domains of subunit C close to the N-terminal domains of two of the peripheral stalks (EG^1 and EG^2). This orientation of subunit C is supported by recent cross-linking data that showed that residues in both the foot and head domains (indicated by *red spacefill* in Fig. 6*A*) are close to subunits E and G in the yeast enzyme (34). The fit of the two conformers also suggests that flexibility of the head domain might explain the limited resolution of the interacting peripheral stalk (EG^2).

Subunit H—Fitting of subunit H (Vma13p) is summarized in Fig. 6, *D–F*. The crystal structure of Vma13p (PDB 1ho8; Fig. 6*D*) was fitted into the electron density at the periphery of the stalk region based on our earlier mapping of the subunit in the bovine V-ATPase (23). The fit places the N-terminal domain of subunit H (H_{nt}) at the very periphery, extending about 2 nm toward the outside. The rest of the subunit seems to provide a link between the bottom of one of the B subunits (via the conserved residues shown in *white spacefill* in Fig. 6*D*) and the N-terminal domain of subunit *a* (see below). This orientation of subunit H puts Pro^{197} (shown in *red spacefill*) close to subunit E (EG^3) as observed by chemical cross-linking (54). The orientation of the C-terminal domain (H_{ct}), however, is inconsistent with cross-linking results (54), which put Asp^{390} (*blue spacefill*) in close proximity to a B subunit and Ser^{381} (*magenta*) to F (cross-links observed in V_1-ATPase only) (54). It has been shown that the two domains of subunit H have separable functions (55), indicating that the linker region around position 354 is flexible and that the two domains of the subunit might adopt different orientations with respect to one another depending on whether the subunit is isolated, bound to V_1, or bound to V_1V_0. We therefore have broken the linker between Thr^{354}–Ser^{355} and placed the C-terminal domain of subunit H independently (keeping the new ends close together) from its N-terminal domain as shown in Fig. 6*F*. This way, the cross-link sites are oriented toward the interior of the complex and there is room for placing the N-terminal domain of subunit *a* ($Vphp1_{nt}$, see below).

The Subunits of the V_0: Subunit d—The structure of subunit *d* (Vma6p) was modeled after the bacterial A/V-ATPase subunit C (PDB 1r5z; ~18% identity over the entire polypeptide). The subunit is folded in three helical domains, which are arranged in a cone-like structure with pseudo 3-fold symmetry. A three-domain density can be seen in the opening of the proteolipid ring in the EM model of the bovine V_0 (22), which fits the crystal structure of the subunit *d* homolog very well (32). A very similar density is present in the model of the intact yeast V-ATPase. We have placed the subunit *d* homology model into the density filling the cytoplasmic opening of the proteolipid ring where it makes contact to the bottom of the density, which we have tentatively assigned as subunits D and F. This is shown in Fig. 7*A*.

Proteolipid Ring—Currently, there is no structure for the ring of V-ATPase subunit *c* (proteolipids *c*, *c*, and *c*″). A crystal structure is available for a ring of 10 V-ATPase-like proteolipids (k_{10}) from *E. hirae* (56) but the subunit *c* (including *c*′ and *c*″) stoichiometry in the eukaryotic V-ATPase is not firmly established. We tried fitting with the k_{10} ring (PDB 2bl2), the c_{11} ring of the *Ilyobacter tartaricus* sodium F-ATPase (PDB 1yce; 57) as well as the modeled c_{12} ring from *E. coli* (12 F-ATPase proteolipids correspond to 6 V-ATPase proteolipids

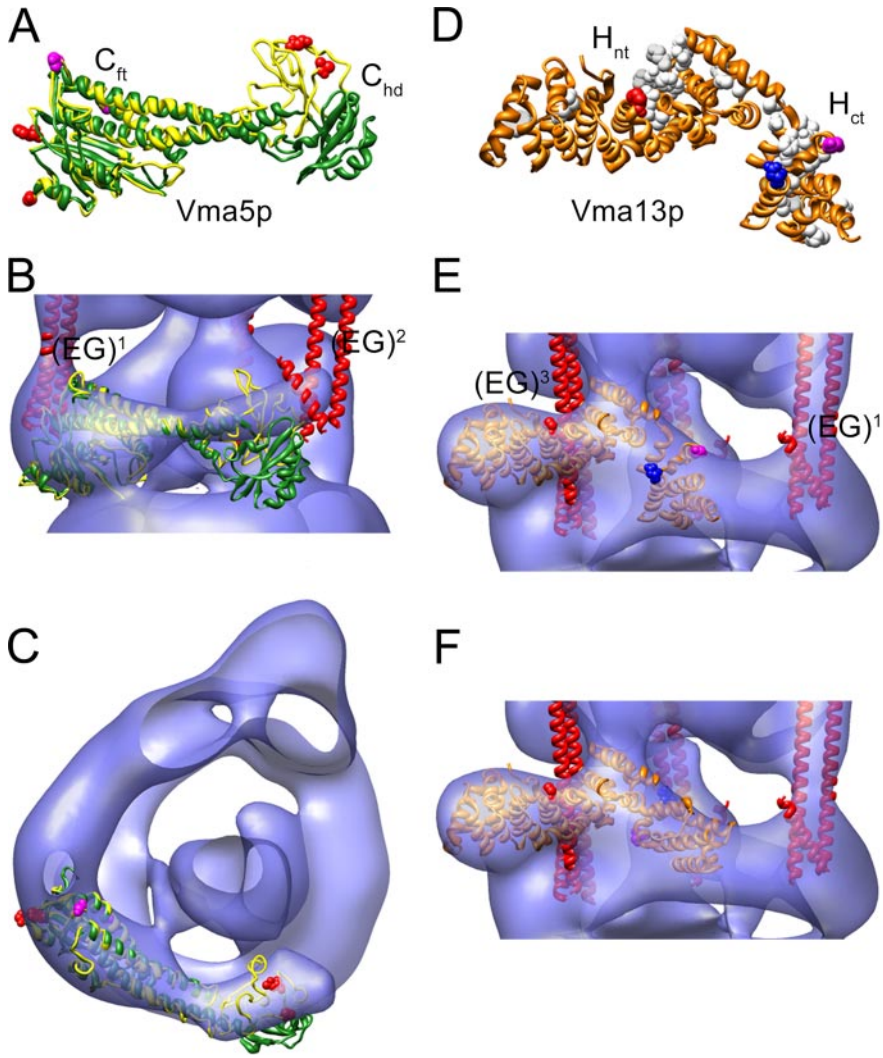

FIGURE 6. **Fitting of subunit C and H crystal structures into the yeast V-ATPase three-dimensional model.** *A*, overlay of the high (*green*) and low (*yellow*) conformers of subunit C (PDB 1u7l; Ref. 42). As can be seen, the foot domains (C_{ft}) match well, whereas the position of the head domains (C_{hd}) varies, indicating some flexibility of the two domains. Coordinates of the low-resolution conformer were kindly provided by Dr. Nathan Nelson. The sites from where cross-linking to EG has been observed (34) are in *red spacefill*. *B* and *C*, fitting of both subunit C conformers into the V-ATPase three-dimensional model reveals a better fit for the low-resolution conformer. *D*, crystal structure of subunit H (PDB 1ho8; Ref. 43) showing an N-terminal domain (H_{nt}) and a C-terminal domain (H_{ct}). Conserved residues are in *white spacefill*. Residues from where cross-links to subunits E, B, and F have been observed (54) are in *red*, *blue*, and *magenta* spacefill, respectively. *E*, fitting of the crystal structure of subunit H into the V-ATPase three-dimensional model. In this orientation, the sites cross-linking to B and F are on the outside. The H_{ct} domain was therefore fitted separately (see *panel F*) in accordance with the independent behavior of the two domains as reported for the yeast enzyme (55).

in terms of the number of transmembrane α helices and there is evidence that eukaryotic V-ATPase proteolipids can form hexameric rings (58)). The density corresponding to the V_0 (Fig. 1, *B3*) can accommodate any of these rings but the stain-filled cavity is more similar in size to the cavity in the k_{10} ring. We therefore decided to use the k_{10} ring for the fit into the model as shown in Fig. 7.

Subunit a—As can be seen, the V_0 is significantly larger than the k_{10} ring. This size difference can be explained by a layer of detergent bound to the exterior surface of the proteolipids (that excludes the negative stain), in addition to the presence of the C-terminal domain of subunit *a* (a_{ct}) bound to the periphery of the ring, which gives the density corresponding to the V_0 its characteristic asymmetry (Fig. 1, *B3*, and Ref. 22). The large cytoplasmic domain of subunit *a* is least well understood. It comprises the N-terminal ~400 residues (and has been shown to interact with or be close to subunits A, EG, H, and C). To accommodate these interactions, we have divided the *a* subunit N-terminal domain (a_{nt}) into a part that emerges from the membrane and goes to the bottom of the V_1 where it makes contact with one of the A subunits and a domain that fills part of the collar-like structure between subunits H and C. This arrangement of a_{nt} is supported by secondary structure and coiled coil prediction as shown in Fig. 7*C* as well as the observed proximity between subunit *a* and C_{ft} (34). As can be seen from Fig. 7*C*, a_{nt} is predicted to contain two long α helices that are folded as a coiled coil. The length of the helices (helix 1, 105–151, ~70 Å; helix 2, 267–328, ~90 Å) and their size fits well as indicated by the schematic drawing in Fig. 7, *A* and *B*. This way, a_{nt} can interact with H, EG, A (connecting density between a_{nt} and one of the A subunits can be seen at a lower contour level; supplemental Fig. S3), and be close enough to the foot of subunit C as observed by the chemical photo-cross-link (34).

DISCUSSION

In this study, we determined a 25-Å resolution three-dimensional structure of the yeast vacuolar ATPase from electron microscopic images of a negatively stained specimen. Overall, the three-dimensional model of the yeast enzyme is very similar to the structural model of the V-ATPase from bovine brain clathrin-coated vesicles (23) (supplemental Fig. S2) except for the presence of two extra densities in the bovine model, which can be explained by two subunits (Hβ and Ac45) not found in yeast. Next, we fitted available crystal structures of isolated subunits and related polypeptides into the three-dimensional electron density, thus generating a pseudo-atomic resolution structural model of the complex. Placement of the individual structures is based on the subunit localization data presented in this study, our earlier electron microscopy data for the yeast- and bovine V-ATPase (reviewed in Ref. 32), and the wealth of structural and biochemical data obtained by others (for a recent review see Ref. 1). The placement of subunits is summarized in supplemental Table S2 and the resulting structural model is presented in Fig. 8 (see

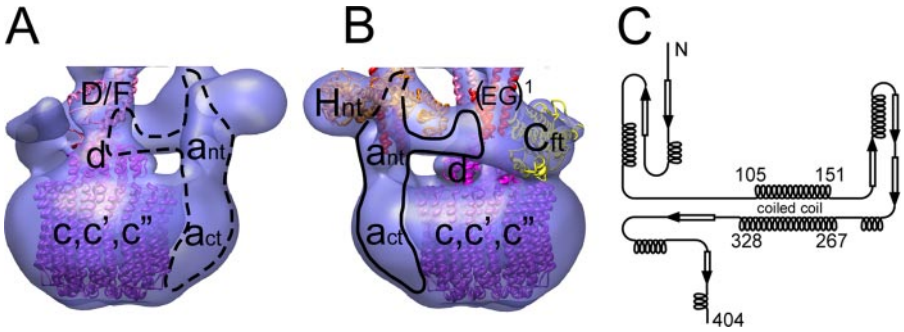

FIGURE 7. **Schematic model of the V_0 domain.** *A*, fitting of the k_{10} proteolipid ring (*purple*; PDB 2bl2), the homology model of yeast subunit *d* (*magenta*; modeled after the homologous subunit C of the bacterial A/V-ATPase (PDB 1r5z)), and the middle domain of the F-ATPase γ subunit (*pink*; PDB 1e79). Currently, there is no structure for subunit D from any species. *B*, proposed arrangement of the N-terminal domain of subunit *a* (a_{nt}). The arrangement is based on secondary structure and coiled coil prediction (EXPASY) as shown in *panel C*. For details, see text.

supplemental Fig. S4 for a ribbon diagram representation of the model).

Proton pumping V-ATPase is assembled from a water-soluble ATP hydrolysis driven rotary molecular motor, a membrane-bound proton pumping turbine, and regulatory subunits that provide a structural link between the two active domains. The ATPase domain consists of a trimer of heterodimers, each heterodimer made of a catalytic A- and non-catalytic B subunit. Although V-ATPase B subunit has a similar size compared with its F-ATPase counterpart (the α subunit), the V-ATPase A subunit is about 10 kDa larger compared with F-ATPase β subunit due to a ~90 amino acid insertion near its N terminus (non-homologous region). Earlier, we had speculated that the knob-like densities seen at the top periphery of the V_1-domain (see Fig. 1*A*, *medium arrows*) were formed by these 90 amino acid insertions into the A subunit, an assumption now supported by the antibody labeling (Fig. 2*A*) as well as the recent x-ray crystal structure of the archaeal ATP synthase A subunit (50) that showed the non-homologous region at the position of the knob-shaped densities in the EM model (Fig. 4*C*). Interestingly, Shao and Forgac (59) recently reported that the individually expressed yeast subunit A non-homologous region (Pro^{144}–Pro^{233}) was able to pull down the V_0 domain in immunoprecipitation experiments, and the authors speculated that the interaction was via the cytoplasmic domain of subunit *a*, consistent with an earlier report of a subunit a_{nt} subunit A interaction (60). Although the EM model of the yeast V-ATPase shows a bridge of density connecting the putative N-terminal domain of subunit *a* to the bottom of subunit A (see supplemental Fig. S3), the limited resolution does not allow us to describe the interaction of the two subunits with sufficient detail to say whether a domain of subunit *a* reaches all the way up to contact the non-homologous region.

The rotary ATPase motor and the proton turbine in both F- and V-ATPase are coupled by central and peripheral stalk domains. The function of the peripheral stalk is to resist the torque generated during rotation of the central stalk. In F-ATPase, the single peripheral stalk contains the δ subunit and the soluble domains of the *b* subunits (subunit nomenclature of the *E. coli* enzyme (61)). In the V-ATPase on the other hand, the peripheral stalk domain is composed of three peripheral stalks (47) (EG^1, EG^2, and EG^3, see Fig. 5) and several polypeptides that have no counterparts in the F-ATPase (subunits H, C, and the N-terminal domain of subunit *a*).

As mentioned under the Introduction, the proton pumping activity of yeast V-ATPase is tightly regulated by a reversible dissociation/re-association mechanism in which the active holoenzyme dissociates into a cytoplasmic V_1 domain that is unable to hydrolyze MgATP and a membrane-bound V_0 domain that is impermeable to protons (19, 20). A similar mechanism has not been demonstrated in F-ATPase suggesting that at least part of the above mentioned regulatory subunits are involved in the mechanism of reversible dissociation in V-ATPase. In yeast, enzyme dissociation is induced by glucose withdrawal by an as yet unknown mechanism (19).

The only subunit that does not co-purify with either V_0 or V_1 after disassembly is subunit C, pointing to a role of this subunit in the mechanism of reversible dissociation-reassociation (62). In our structural model (Fig. 8), subunit C is interacting with the N termini of peripheral stalks EG^1 and EG^2 via its foot and head domains, respectively (Fig. 6). Peripheral stalk EG^1 also interacts with the N-terminal domain of subunit *a*, thereby providing an indirect link between stator EG^2, subunit C, and the membrane domain of the complex (Fig. 7). Subunit H on the other hand seems to interact with only one of the stators (EG^3) together with the N-terminal domain of subunit *a*. It has been shown that V-ATPase is able to assemble on the vacuolar membrane in the absence of subunit H and that the resulting complex is inactive (63). Thus, subunit H appears non-essential for a structural interaction between V_1 and V_0 in the absence of catalytic turnover. Deletion of subunit C on the other hand results in vacuolar membranes essentially devoid of assembled V-ATPase complex. This indicates that the interactions of the peripheral stalks with the C-subunit are important and that breaking one or both of these interactions might ultimately lead to enzyme disassembly.

As can be seen from Fig. 1, *A2*, the region where the peripheral stator EG^2 is interacting with the head domain of subunit C (C_{hd}) is poorly resolved, indicating flexibility in this region of the complex. Two conformations of subunit C have been observed by x-ray crystallography and the two crystal forms differ in the orientation of the head with respect to the foot domain (42). As shown in Fig. 6, only one of the conformers provides a good fit to the EM derived three-dimensional model, and it is possible that exchange between these two conformations is involved in initiating enzyme dissociation. What may be causing subunit C to change conformation upon glucose withdrawal? For instance, it has been shown that subunit C undergoes a conformational change upon binding of calcium nucleotide *in vitro* (64) and it is possible that a change in the ATP/ADP ratio upon glucose withdrawal favors the high-resolution conformation of subunit C. Another possible mechanism involves phosphorylation of subunit C, which has been shown

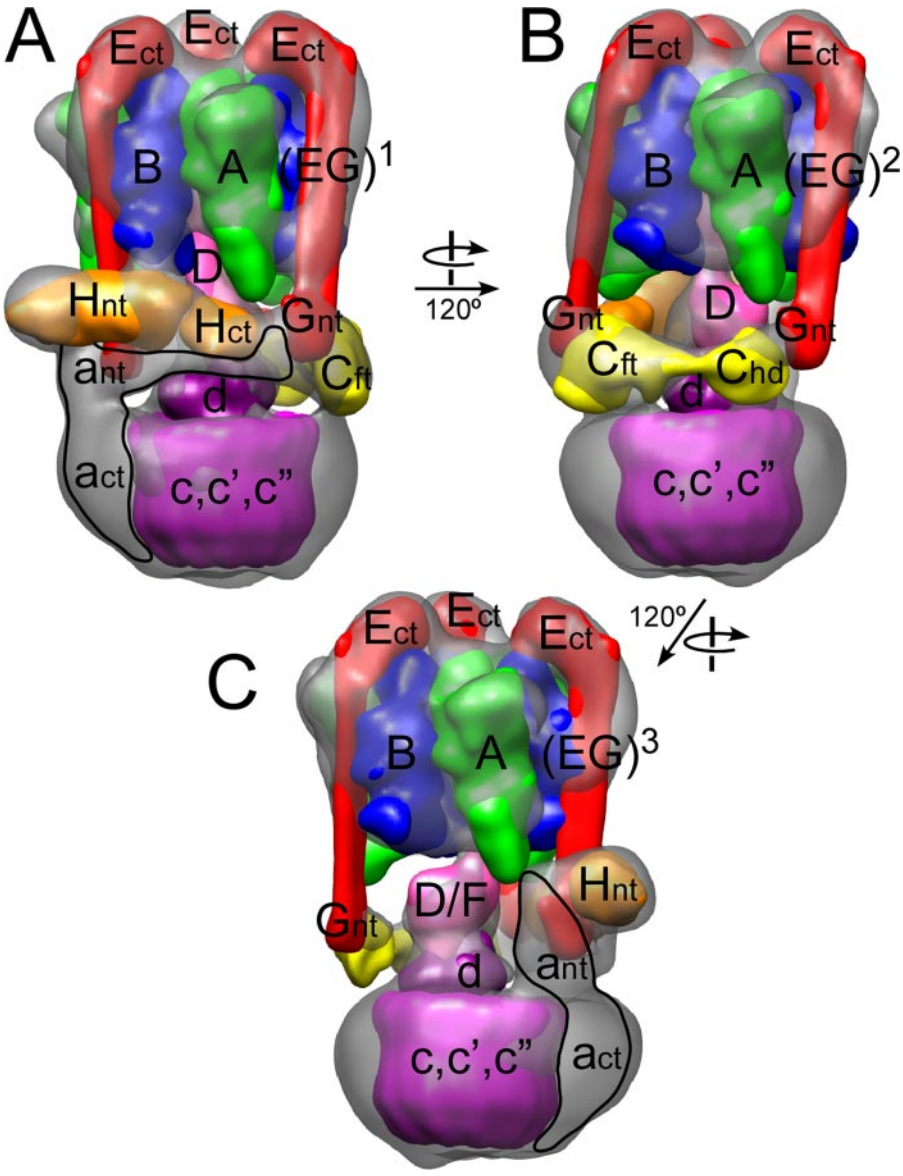

FIGURE 8. **Model of the subunit arrangement in the yeast V-ATPase.** The crystal structures used for fitting were low pass filtered to 20-Å resolution and rendered as three-dimensional volumes before fitting into the electron density three-dimensional envelope of the V-ATPase. The structures used for fitting were the homology models of the yeast A (*green*) and B (*blue*) subunits (modeled based on PDB 1vdc and PDB 2c61, respectively), the γ subunit from mitochondrial F_1-ATPase (PDB 1e79; *pink*), the H and C subunits from yeast V-ATPase (*H*, PDB 1ho8, *orange*; *C*, Ref. 42, *yellow*), the structural model of the EG heterodimer (*red*; containing PDB 2dma), the homology model of yeast subunit *d* (*magenta*; modeled after bacterial V-ATPase C subunit, PDB 1r5z), and the k_{10} proteolipid ring (PDB 2bl2; *purple*). No representative structure is available for the N-terminal domain of the *a* subunit. A structure for subunit F is available (PDB 2d00) but the small size of the subunit (~11 kDa) makes docking unreliable. Subunit *e* (Vma9p; 14) is not included in the model as there is insufficient information regarding its binding location.

to occur upon stimulation of V-ATPase assembly in insect salivary glands (65).

The less well resolved electron density involving the second peripheral stalk (EG^2) suggests that the interaction between C_{hd} and EG^2 represents the "weak link" in the V_1-V_0 interaction and that breaking or destabilizing that link, triggered by glucose withdrawal, may initiate disassembly. A crucial part of the dissociation mechanism seems to be the torque generated during ATP hydrolysis as it has been observed that controlled disassembly of yeast V-ATPase requires active enzyme. For example, it has been shown that the inhibitor concanamycin is able to prevent enzyme disassembly *in vivo* (66) and that the presence of MgATP is required to dissociate V_1V_0 holoenzyme *in vitro* (67). Further evidence that the interaction of C_{hd} is involved in dissociation comes from mutagenesis studies conducted with subunit G. It has been shown that a mutation in the N terminus of the subunit (Arg^{25} to Leu or Ala) leads to an enzyme complex that shows a reduced tendency to dissociate with no significant change in activity (68). From cross-linking (34), it was shown that the head domain of subunit C is close to subunit G (in the EG^2 peripheral stalk) and it is possible that the mutation in the N terminus of subunit G leads to a stronger interaction of EG^2 with C_{hd}, thus preventing efficient disassembly. Domain mapping experiments on the other hand showed that the interaction of the peripheral stalk with subunit C involves the N-terminal residues of subunit E (69). These data together with the subunit G mutagenesis study indicates that the N termini of both subunits E and G are directly in contact with subunit C and it is possible that subunit E is mostly responsible for the interaction with one end of subunit C (*e.g.* the foot), whereas subunit G provides most of the binding energy to the other end (the head).

Recently, it has been shown that EG heterodimer binds subunit C with high affinity and 1:1 stoichiometry *in vitro* (70). We speculate that the *in vitro* interaction of EG with subunit C is via the foot domain and that the interaction of the EG^2 heterodimer with the head domain of subunit C occurs only in the assembled V-ATPase complex. When dissociation occurs, subunit C appears to be modified and/or sequestered by another cellular factor, as it is not co-purified with V_1-ATPase (71), even though recombinant subunit C is able to bind V_1 *in vitro* (65). It has been shown that efficient *de novo* assembly and re-assembly of the complex upon glucose addition to glucose-deprived cells requires a chaperone complex called RAVE (72), a three protein assembly that is able to bind both the V_1 via the EG subunits and subunit C. This suggests that during re-assembly, subunit C is delivered to the V_1 domain in a conformation that is able to bind two EG heterodimers, thus providing enough binding energy to form a

stable V_1-V_0 interface. Interestingly, dissociation does not require the RAVE complex (72), therefore this process may occur by a different mechanism.

It is also of interest in this regard that the related bacterial A/V-ATPase has only two peripheral stalks, which are indirectly connected to the membrane domain via an interaction with the N-terminal domain of the subunit corresponding to subunit *a* in yeast (subunit I) (73). Recently it has been shown that the N-terminal domain of subunit I of the sodium V-ATPase from *E. hirae*, much like subunit C (Ref. 70 and see above), is able to bind a heterodimer of the corresponding peripheral stalk subunits with 1:1 stoichiometry (74). The small angle x-ray scattering solution structure of the resulting complex showed both components (NtpE-NtpF heterodimer and subunit I N-terminal domain) as elongated molecules arranged in an "L" shaped fashion, consistent with the proposed structure of the yeast V-ATPase *a* subunit N-terminal domain as shown in Fig. 7. Bacterial A/V-ATPase has no V-ATPase subunit C equivalent and as of now there is no report that the bacterial enzyme is regulated by reversible dissociation, again pointing to the proposed role of subunit C and stator EG^2 in the regulation of yeast V-ATPase.

Subunit H plays a dual role in the function of the V-ATPase complex: in the intact enzyme, subunit H is required for MgATPase activity (63), whereas in the free V_1, the subunit is responsible for silencing the MgATPase activity (71). It has been shown that the N- and C-terminal domains of subunit H do not have to be connected for assembly of an active complex (55), indicating some flexibility of the two domains with respect to one another. Lack of the N-terminal domain prevents assembly and leads to a destabilization of subunit E, suggesting that H_{nt} interacts with the V_1 domain. The C-terminal domain on the other hand, when expressed alone is found to be associated with the vacuolar membrane, suggesting that it is interacting with a subunit of the V_0, most likely the N-terminal domain of subunit *a*. Overall, this interaction scheme of subunit H domains is consistent with the fitting of the subunit into the electron density map of the V-ATPase as shown in Fig. 6. This orientation of subunit H is also supported by chemical cross-linking and two-hybrid experiments that place the subunit in close proximity to subunits B and E (23, 54, 75). Furthermore, the fit of subunit H places its N-terminal domain at the periphery of the complex, consistent with the observation that this part of the subunit can be deleted without effect on assembly (63).

In the related F-ATPase, the single peripheral stalk is attached to the ATPase domain via interaction of the N-terminal domain of the δ subunit with the N-terminal 22 residues of one of the α subunits (*E. coli* nomenclature) (76). Although the C-terminal domain of the F-ATPase δ subunit is similar to the C-terminal domain of V-ATPase subunit E (44), their N-terminal domains are different. We have argued earlier that in order to move from the single peripheral stalk of the F-ATPase to the three stalks in the V-ATPase, the N-terminal domain of the δ subunit had to be eliminated as there is room for only one δ subunit on top of the F_1 (44). The C-terminal domain of δ on the other hand was fused to a F-ATPase *b* subunit-like polypeptide to form the V-ATPase E subunit. There is limited but significant sequence homology between the F-ATPase *b* subunit soluble domain and the V-ATPase G subunit (77), and it is possible that the N-terminal domains of both E and G subunits share a common origin with the bacterial F-ATPase *b* subunits. How the interaction of the EG heterodimers with the A_3B_3 hexamer is mediated is currently unknown, but at least in yeast V-ATPase the interaction appears to be of sufficient affinity to allow isolation of a V_1-ATPase complex with all three EG dimers bound (47). It has been shown that both E and G subunits are in close proximity to the periphery of the B subunits for its entire length (53) suggesting that the interaction of the peripheral stalks with the A_3B_3 domain is different compared with the interaction of the $b_2\delta$ peripheral stalk with the F-ATPase domain, where most, if not all, of the binding interaction is localized to the N-terminal 22 residues of the α subunit (76). The tandem mass spectrometry data presented here suggest that both subunits E and G interact with the catalytic core of the V_1 as subcomplexes lacking either subunit E or (to a lesser degree) G can be detected.

In summary, we have generated a detailed structural model of the eukaryotic V-ATPase complex using a 25-Å resolution electron microscopy derived model of the complex as a scaffold to fit the available high resolution structures of V-ATPase subunits and related polypeptides. The model predicts several interactions within the stator-forming subunits and subunit domains that can be tested in future experiments. Knowledge of the high resolution structural details of the V-ATPase stator domain will be essential for a more complete understanding of the mechanism of regulation of this important enzyme complex.

REFERENCES

1. Forgac, M. (2007) *Nat. Rev. Mol. Cell. Biol.* **8,** 917–929
2. Kane, P. M. (2006) *Microbiol. Mol. Biol. Rev.* **70,** 177–191
3. Marshansky, V., and Futai, M. (2008) *Curr. Opin. Cell Biol.*, **20,** 415–426
4. Alper, S. L. (2002) *Annu. Rev. Physiol.* **64,** 899–923
5. Kornak, U., Schulz, A., Friedrich, W., Uhlhaas, S., Kremers, B., Voit, T., Hasan, C., Bode, U., Jentsch, T. J., and Kubisch, C. (2000) *Hum. Mol. Genet.* **9,** 2059–2063
6. Visentin, L., Dodds, R. A., Valente, M., Misiano, P., Bradbeer, J. N., Pneta, S., Liang, X., Gowen. M., and Farina, C. (2000) *J. Clin. Investig.* **106,** 309–318
7. Sun-Wada, G. H., Toyomura, T., Murata, Y., Yamamoto, A., Futai. M., and Wada, Y. (2006) *J. Cell Sci.* **119,** 4531–4540
8. Smith, A. N., Skaug, J., Choate, K. A., Nayir, A., Bakkaloglu, A., Ozen, S., Hulton, S. A., Al-Sabban, E. A., Lifton, R. P., Scherer, S. W., and Karet, F. E. (2000) *Nat. Genet.* **26,** 71–75
9. Hahn, H., Kang, H. G., Ha, I. S., Cheong, H. I., and Choi, Y. (2003) *Am. J. Kidney Dis.* **41,** 238–243
10. Sennoune, S. R., and Martinez-Zaguilan, R. (2007) *J. Bioenerg. Biomembr.* **39,** 349–355
11. Geyer, M., Yu, H., Mandic, R., Linnemann, T., Zheng, Y. H., Fackler, O. T., and Peterlin, B. M. (2002) *J. Biol. Chem.* **277,** 28521–28529
12. Ludwig, J., Kerscher, S., Brandt, U., Pfeiffer, K., Getlawi, F., Apps, D. K., and Schägger, H. (1998) *J. Biol. Chem.* **273,** 10939–10947
13. Merzendorfer, H., Huss, M., Schmid, R., Harvey, W. R., and Wieczorek, H. (1999) *J. Biol. Chem.* **274,** 17372–17378
14. Sambade, M., and Kane, P. M. (2004) *J. Biol. Chem.* **279,** 17361–17365
15. Wilkens, S. (2005) *Adv. Protein Chem.* **71,** 345–382
16. Imamura, H., Nakano, M., Noji, H., Muneyuki, E., Ohkuma, S., Yoshida, M., and Yokoyama, K. (2003) *Proc. Natl. Acad. Sci. U. S. A.* **100,** 2312–2315
17. Hirata, T., Iwamoto-Kihara, A., Sun-Wada, G. H., Okajima, T., Wada, Y.,

and Futai, M. (2003) *J. Biol. Chem.* **278,** 23714–23719
18. Yokoyama, K., Nakano, M., Imamura, H., Yoshida, M., and Tamakoshi, M. (2003) *J. Biol. Chem.* **278,** 24255–24258
19. Kane, P. M. (1995) *J. Biol. Chem.* **270,** 17025–17032
20. Sumner, J. P., Dow, J. A., Earley, F. G., Klein, U., Jäger, D., and Wieczorek, H. (1995) *J. Biol. Chem.* **270,** 5649–5653
21. Wilkens, S., Vasilyeva, E., and Forgac, M. (1999) *J. Biol. Chem.* **274,** 31804–31810
22. Wilkens, S., and Forgac, M. (2001) *J. Biol. Chem.* **276,** 44064–44068
23. Wilkens, S., Inoue, T., and Forgac, M. (2004) *J. Biol. Chem.* **279,** 41942–41949
24. Grüber, G., Radermacher, M., Ruiz, T., Godovac-Zimmermann, J., Canas, B., Kleine-Kohlbrecher, D., Huss, M., Harvey, W. R., and Wieczorek, H. (2000) *Biochemistry* **39,** 8609–8616
25. Radermacher, M., Ruiz, T., Wieczorek, H., and Grüber, G. (2001) *J. Struct. Biol.* **135,** 26–37
26. Rizzo, V. F., Coskun, U., Radermacher, M., Ruiz, T., Armbrüster, A., and Grüber, G. (2003) *J. Biol. Chem.* **278,** 270–275
27. Li, Z., and Zhang, X. (2004) *Planta* **219,** 948–954
28. Domgall, I., Venzke, D., Lüttge, U., Ratajczak, R., and Böttcher, B. (2002) *J. Biol. Chem.* **277,** 13115–13121
29. Venzke, D., Domgall, I., Kocher, T., Féthière, J., Fischer, S., and Böttcher, B. (2005) *J. Mol. Biol.* **349,** 659–669
30. Zhang, Z., Charsky, C., Kane, P. M., and Wilkens, S. (2003) *J. Biol. Chem.* **278,** 47299–47306
31. Zhang, Z., Inoue, T., Forgac, M., and Wilkens, S. (2006) *FEBS Lett.* **580,** 2006–2010
32. Wilkens, S., Zhang, Z., and Zheng, Y. (2005) *Micron* **36,** 109–126
33. Ohira, M., Smardon, A. M., Charsky, C. M., Liu, J., Tarsio, M., and Kane, P. M. (2006) *J. Biol. Chem.* **281,** 22752–22760
34. Inoue, T., and Forgac, M. (2005) *J. Biol. Chem.* **280,** 27896–27903
35. Sobott, F. (2002) *Anal. Chem.* **74,** 1402–1407
36. van den Heuvel, R. H. H. (2006) *Anal. Chem.* **78,** 7473–7483
37. Lorenzen, K., Versluis, C., van Duijn, E., van den Heuvel, R. H. H., and Heck, A. J. R. (2007) *Int. J. Mass Spectrom.* **268,** 198–206
38. Lüdtke, S. J., Baldwin, P. R., and Chiu, W. (1999) *J. Struct. Biol.* **128,** 82–97
39. van Heel, M., Harauz, G., Orlova, E. V., Schmidt, R., and Schatz, M. (1996) *J. Struct. Biol.* **116,** 17–24
40. Dube, P., Tavares, P., Lurz, R., and van Heel, M. (1993) *EMBO J.* **12,** 1303–1309
41. Böttcher, B., Wynne, S. A., and Crowther, R. A. (1997) *Nature* **386,** 88–91
42. Drory, O., Frolow, F., and Nelson, N. (2004) *EMBO Rep.* **5,** 1–5
43. Sagermann, M., Stevens, T. H., and Matthews, B. W. (2000) *Proc. Natl. Acad. Sci. U. S. A.* **98,** 7134–7139
44. Kish-Trier, E., Briere, L. A., Dunn, S. D., and Wilkens, S. (2008) *J. Mol. Biol.* **375,** 673–685
45. Wriggers, W., Milligan, R. A., and McCammon, J. A. (1999) *J. Struct. Biol.* **125,** 185–195
46. Pettersen, E. F., Goddard, T. D., Huang, C. C., Couch, G. S., Greenblatt, D. M., Meng, E. C., and Ferrin, T. E. (2004) *J. Comput. Chem.* **25,** 1605–1612
47. Kitagawa, N., Mazon, H., Heck, A. J., and Wilkens, S. (2008) *J. Biol. Chem.* **283,** 3329–3337
48. Sharon, M., and Robinson, C. V. (2007) *Annu. Rev. Biochem.* **76,** 167–193
49. Lorenzen, K., Vannini, A., Cramer, P., and Heck, A. J. R. (2007) *Structure* **15,** 1237–1245
50. Maegawa, Y., Morita, H., Iyaguchi, D., Yao, M., Watanabe, N., and Tanaka, I. (2006) *Acta Crystallogr. D Biol. Crystallogr.* **62,** 483–488
51. Lokanath, N. K., Matsuura, Y., Kuroishi, C., Takahashi, N., and Kunishima, N. (2007) *J. Mol. Biol.* **366,** 933–944
52. Féthière, J., Venzke, D., Diepholz, M., Seybert, A., Geerlof, A., Gentzel, M., Wilm, M., and Böttcher, B. (2004) *J. Biol. Chem.* **279,** 40670–40676
53. Arata, Y., Baleja, J. D., and Forgac, M. (2002) *J. Biol. Chem.* **277,** 3357–3363
54. Jefferies, K. C., and Forgac, M. (2008) *J. Biol. Chem.* **283,** 4512–4519
55. Liu, M., Tarsio, M., Charsky, C. M., and Kane, P. M. (2005) *J. Biol. Chem.* **280,** 36978–36985
56. Murata, T., Yamamato, I., Kakinuma, Y., Leslie, A. G., and Walker, J. E. (2005) *Science* **308,** 654–659
57. Meier, T., Polzer, P., Diedrichs, K., Welte, W., and Dimroth, P. (2005) *Science* **308,** 659–662
58. Clare, D. K., Orlova, E. V., Finbow, M. A., Harrison, M. A., Findlay, J. B., and Saibil, H. R. (2006) *Structure* **14,** 1149–1156
59. Shao, E., and Forgac, M. (2004) *J. Biol. Chem.* **279,** 48663–48670
60. Landolt-Marticorena, C., Williams, K. M., Correa, J., Chen, W., and Manolson, M. F. (2000) *J. Biol. Chem.* **275,** 15449–15457
61. Dunn, S. D., McLachlin, D. T., and Revington, M. (2000) *Biochim. Biophys. Acta* **1458,** 356–363
62. Curtis, K. K., Francis, S. A., Oluwatosin, Y., and Kane, P. M. (2002) *J. Biol. Chem.* **277,** 8979–8988
63. Ho, M. N., Hirata, R., Umemoto, N., Ohya, Y., Takatsuki, A., Stevens, T. H., and Anraku, Y. (1993) *J. Biol. Chem.* **268,** 18286–18292
64. Armbrüster, A., Hohn, C., Hermesdorf, A., Schumacher, K., Börsch, M., and Grüber, G. (2005) *FEBS Lett.* **579,** 1961–1967
65. Voss, M., Vitavska, O., Walz, B., Wieczorek, H., and Bauman, O. (2007) *J. Biol. Chem.* **282,** 33735–33742
66. Parra, K. J., and Kane, P. M. (1998) *Mol. Cell. Biol.* **18,** 7064–7074
67. Huss, M., and Wieczorek, H. (2007) *FEBS Lett.* **581,** 5566–5572
68. Charsky, C. M., Schumann, N. J., and Kane, P. M. (2000) *J. Biol. Chem.* **275,** 37232–37239
69. Jones, R. P., Durose, L. J., Findlay, J. B., and Harrison, M. A. (2005) *Biochemistry* **44,** 3933–3941
70. Féthière, J., Venzke, D., Madden, D. R., and Böttcher, B. (2005) *Biochemistry* **44,** 15906–15914
71. Parra, K. J., Keenan, K. L., and Kane, P. M. (2000) *J. Biol. Chem.* **275,** 21761–21767
72. Smardon, A., and Kane, P. M. (2007) *J. Biol. Chem.* **282,** 26185–26194
73. Esteban, O., Bernal, R. A., Donohoe, M., Videler, H., Sharon, M., Robinson, C. V., and Stock, D. (2008) *J. Biol. Chem.* **283,** 2595–2603
74. Yamamoto, M., Unzai, S., Saijo, S., Ito, K., Mizutani, K., Suno-Ikeda, C., Yabuki-Miyata, Y., Terada, T., Toyama, M., Shirouzu, M., Kobayashi, T., Kakinuma, Y., Yamato, I., Yokoyama, S., Iwata, S., and Murata, T. (2008) *J. Biol. Chem.* **283,** 19422–19431
75. Lu, M., Vergara, S., Zhang, L., Holliday, L. S., Aris, J., and Gluck, S. L. (2002) *J. Biol. Chem.* **277,** 38409–38415
76. Wilkens, S., Borchardt, D., Weber, J., and Senior, A. E. (2005) *Biochemistry* **44,** 11786–11794
77. Supekova, L., Sbia, M., Supek, F., Ma, Y., and Nelson, N. (1996) *J. Exp. Biol.* **199,** 1147–1156